JCTC Journal of Chemical Theory and Computation

Article

pubs.acs.org/JCTC

Steady-State Electrodiffusion from the Nernst–Planck Equation Coupled to Local Equilibrium Monte Carlo Simulations

Dezső Boda*,† and Dirk Gillespie‡

†Department of Physical Chemistry, University of Pannonia, P.O. Box 158, H-8201 Veszprém, Hungary

‡Department of Molecular Biophysics and Physiology, Rush University Medical Center, Chicago, Illinois 60612, United States

Supporting Information

ABSTRACT: We propose a procedure to compute the steady-state transport of charged particles based on the Nernst–Planck (NP) equation of electrodiffusion. To close the NP equation and to establish a relation between the concentration and electrochemical potential profiles, we introduce the Local Equilibrium Monte Carlo (LEMC) method. In this method, Grand Canonical Monte Carlo simulations are performed using the electrochemical potential specified for the distinct volume elements. An iteration procedure that self-consistently solves the NP and flux continuity equations with LEMC is shown to converge quickly. This NP+LEMC technique can be used in systems with diffusion of charged or uncharged particles in complex three-dimensional geometries, including systems with low concentrations and small applied voltages that are difficult for other particle simulation techniques.

1. INTRODUCTION

The purpose of this paper is to present a general methodology to study steady-state diffusive transport of charged particles on the basis of the Nernst–Planck (NP) equation of electrodiffusion:

$$\mathbf{j}^{\alpha}(\mathbf{r}) = -\frac{1}{kT} D^{\alpha}(\mathbf{r})\, c^{\alpha}(\mathbf{r})\, \nabla\mu^{\alpha}(\mathbf{r}) \tag{1}$$

where T is the temperature, k is Boltzmann's constant, $D^{\alpha}(\mathbf{r})$ is the diffusion coefficient profile ($\alpha = 1, ..., M$ refers to diffusing species), $c^{\alpha}(\mathbf{r})$ is the density (concentration) profile, and $\mathbf{j}^{\alpha}(\mathbf{r})$ is the particle flux density that must satisfy the continuity equation

$$\nabla\cdot\mathbf{j}^{\alpha}(\mathbf{r}) = 0 \tag{2}$$

The electrochemical potential is given by

$$\mu^{\alpha}(\mathbf{r}) = \mu_c^{\alpha}(\mathbf{r}) + z^{\alpha}e\Phi(\mathbf{r}) \tag{3}$$

and is divided into the chemical, $\mu_c^{\alpha}(\mathbf{r})$, and electrical, $z^{\alpha}e\Phi(\mathbf{r})$, work done in bringing an ion from a standard state to the specified concentration and electrical potential (z^{α} is the valence, e is the electronic charge, and $\Phi(\mathbf{r})$ is the mean electrical potential). Because the chemical work and the electrical work cannot be separated experimentally, the electrochemical potential must be used as a variable. In theories and simulations, however, $\Phi(\mathbf{r})$ can be computed so $\mu_c^{\alpha}(\mathbf{r})$ can be obtained from eq 3 if $\mu^{\alpha}(\mathbf{r})$ is known.

The NP equation contains two thermodynamic variables ($c^{\alpha}(\mathbf{r})$ and $\mu^{\alpha}(\mathbf{r})$), and a closure is needed that defines the relation between these two functions. Because the methodology works on the basis of a well-defined molecular model (that determines the Hamiltonian of the system unambiguously), this relation must be provided by statistical mechanics. Here, we propose to use Monte Carlo (MC) simulations to couple the electrochemical potentials and the concentrations.

Before detailing our method, we describe past closures. The Poisson–Boltzmann (PB) theory is widely used to compute the relation between $c^{\alpha}(\mathbf{r})$ and $\mu^{\alpha}(\mathbf{r})$. When coupled to the NP equation and solved self-consistently (with Poisson's equation also satisfied), it is called the Poisson–Nernst–Planck (PNP) theory.[1] In this model, ions are represented as point charges interacting with the mean electric field, while the solvent is represented as a dielectric background. The applicability of this approach is limited to dilute electrolyte solutions because this theory does not take the size of the ions and ionic correlations into account.

To handle these correlations and go beyond the mean field level of the PB theory, advanced statistical mechanical theories are needed. Gillespie et al.,[2] for example, developed a Density Functional Theory (DFT) coupled to the NP equation (PNP/DFT). DFT provides $\{\mu^{\alpha}(\mathbf{r})\}$ from $\{c^{\alpha}(\mathbf{r})\}$, thus establishing the relation between them and providing the closure. However, DFT contains certain approximations, as every theory does. Moreover, it can be applied easily only in one dimension for limited geometries and molecular models.

Therefore, the natural need to use computer simulations to establish the general relation between $\{\mu^{\alpha}(\mathbf{r})\}$ and $\{c^{\alpha}(\mathbf{r})\}$ arises. In this work, we suggest using MC simulations for this purpose. This is novel because the MC method is commonly considered[3,4] to be usable only in global equilibrium where μ^{α} is constant and no voltage is applied.

In this paper, we propose a break with this convention and suggest applying MC simulations locally for small subvolumes (denoted by $\mathcal{D}_i$) of the simulation cell that are assumed to be in local equilibrium (LE). Because subvolume $\mathcal{D}_i$ represents an open system, the natural ensemble of the simulation for this subvolume is the grand canonical (GC) ensemble where the thermodynamic state is characterized by the volume (V_i),

Received: November 8, 2011
Published: January 24, 2012

dx.doi.org/10.1021/ct2007988 | J. Chem. Theory Comput. 2012, 8, 824–829

the electrochemical potentials (μ_i^α), and the temperature (T). Therefore, we introduce the Local Equilibrium Monte Carlo (LEMC) simulation method to simulate a globally nonequilibrium steady-state system with spatially varying electrochemical potential by applying separate Grand Canonical Monte Carlo (GCMC) simulations for the separate subvolumes. Our procedure of computing flux with the NP equation and using LEMC for closure will be denoted by NP+LEMC.

The use of LEMC in the NP equation is actually a natural extension of previous applications of NP. The NP equation is a phenomenological relationship between the flux, the concentrations, and the electrochemical potentials. All of the closures of which we are aware have used equilibrium formulations (be it PB, DFT, or something else) to connect $c^\alpha(\mathbf{r})$ and $\mu^\alpha(\mathbf{r})$, making the ansatz that they are connected through the same formalism at and away from equilibrium.[5−8] Here, we propose GCMC as a closure. It is both accurate (up to statistical error)—and by its very nature more accurate than other closures for the same molecular model—and, we show here, computes quickly enough to be useful for many applications.

Using MC in nonequilibrium situations is not new. (1) Both Kinetic Monte Carlo (KMC)[9−13] and Dynamical Monte Carlo (DMC)[14,15] use stochastic MC steps, although in different ways, to study dynamical phenomena directly (a more detailed discussion will be given in the Conclusions). (2) In the dual control cell method,[16] the two baths between which particle transport occurs is simulated by GCMC simulations. The assumption that makes this possible is that these two subsystems are close to equilibrium; therefore, they can be treated with a simulation method designed for equilibrium. The system between the two control cells is still simulated with molecular dynamics (MD),[16,17] Brownian dynamics (BD),[18] or DMC.[14,15] Here, we generalize this idea and extend the GCMC simulations to the entire simulation cell.

The $\{\mu^\alpha(\mathbf{r})\}$ and $\{c^\alpha(\mathbf{r})\}$ functions are characterized by discretized variables denoted by $\{\mu_i^\alpha\}$ and $\{c_i^\alpha\}$, where $i = 1, ..., N$, with N being the number of subvolumes in the simulation domain. The input quantities of an LEMC simulation are the electrochemical potential values, $\{\mu_i^\alpha\}$, in the subvolumes. The output quantities of an LEMC simulation are the concentration values, $\{c_i^\alpha\}$, in the subvolumes. The discretized values of the concentration and the electrochemical potential are assigned to the $\mathbf{r}_i$ centers of the subvolumes: $c^\alpha(\mathbf{r}_i) = c_i^\alpha$ and $\mu^\alpha(\mathbf{r}_i) = \mu_i^\alpha$. The values of these functions in intermediate points, and, therefore, the $\mu^\alpha(\mathbf{r})$ and $c^\alpha(\mathbf{r})$ functions can be obtained from linear interpolation.

Substituting these functions and the $D^\alpha(\mathbf{r})$ diffusion coefficient profile (which must be provided by the user) into the NP equation, the flux density, $\mathbf{j}^\alpha(\mathbf{r})$, can be calculated. There is no guarantee that even an intelligent guess for the $\mu^\alpha(\mathbf{r})$ profiles provides flux densities that satisfy the conservation of mass, e.g., the continuity equation (eq 2). The electrochemical potentials, therefore, must be changed iteratively until we obtain $c^\alpha(\mathbf{r})$ and $\mu^\alpha(\mathbf{r})$ profiles that, in turn, produce flux densities (through the NP equation) that satisfy eq 2. This iteration procedure, in addition to the idea of LEMC, is the other main contribution of this work.

2. LOCAL EQUILIBRIUM MONTE CARLO METHOD

In the LEMC method, we apply independent particle insertion steps into uniformly generated positions $\mathbf{r}$ in the various subdomains $\mathcal{D}_i$ and deletions of uniformly chosen particles from a subdomain. The factor governing the acceptance of the step is

$$p_{i,\chi}^{\alpha}(\mathbf{r}) = \frac{N_i^{\alpha}!V_i^{\chi}}{(N_i^{\alpha}+\chi)!}\exp\left(-\frac{\Delta U(\mathbf{r}) - \chi\mu_i^{\alpha}}{kT}\right) \tag{4}$$

where N_i^α is the number of particles of species α in subvolume $\mathcal{D}_i$ before insertion/deletion, $\chi = 1$ for insertion, and $\chi = -1$ for deletion, V_i is the volume of $\mathcal{D}_i$, and $\Delta U(\mathbf{r})$ is the energy change associated with the insertion or deletion of the particle in/from position $\mathbf{r}$. In the Metropolis sampling, the acceptance probability is $\min[1, p_{i,\chi}^\alpha(\mathbf{r})]$. Insertions and deletions are attempted with equal probability. Acceptance of particle displacements from position $\mathbf{r}$ in subvolume $\mathcal{D}_i$ to position $\mathbf{r}'$ in subvolume $\mathcal{D}_j$ is governed by the factor

$$p_{i\to j}^{\alpha}(\mathbf{r},\mathbf{r}') = \exp\left(-\frac{\Delta U(\mathbf{r},\mathbf{r}') - (\mu_j^{\alpha} - \mu_i^{\alpha})}{kT}\right) \tag{5}$$

The energy change, $\Delta U(\mathbf{r}, \mathbf{r}')$, contains the ion's interaction with an applied potential, $z^\alpha e\Phi^{\text{appl}}(\mathbf{r})$, which is the solution of Laplace's equation, $\nabla^2\Phi^{\text{appl}}(\mathbf{r}) = 0$, with the prescribed Dirichlet boundary conditions on the boundary of the simulation domain. It is important to note that $\mathbf{r}$ and $\mathbf{r}'$ are not restricted to a lattice and can be anywhere within $\mathcal{D}_i$ and $\mathcal{D}_j$, respectively.

The separate LEMC simulations for the various subvolumes are coupled through the temperature and the energy change, ΔU, that contains not only the interaction energies between particles in subvolume $\mathcal{D}_i$ but also the effect of particles outside this subvolume. The interactions with these particles can be considered as an external "constraint" on the particles in subvolume $\mathcal{D}_i$. This "constraint", of course, continuously changes as the simulation evolves.

The mean electrical potential profile $\Phi(\mathbf{r})$ is computed in the simulation "on the fly" by using the inserted ions as test charges. The electrical potentials computed at the positions of the inserted ions are averaged over the subvolume. The electrical potential obtained for subvolume $\mathcal{D}_i$ is assigned to the $\mathbf{r}_i$ center of the subvolume: $\Phi_i = \Phi(\mathbf{r}_i)$.

The discrete values $\{c_i^\alpha\}$ and $\{\mu_i^\alpha\}$ can be used to compute the functions $\{c^\alpha(\mathbf{r})\}$ and $\{\mu^\alpha(\mathbf{r})\}$ at any $\mathbf{r}$ by interpolation. The flux density, $\{\mathbf{j}^\alpha(\mathbf{r})\}$, then can be computed at any position in the simulation domain from the NP equation (eq 1).

3. ITERATION PROCESS ON THE BASIS OF THE CONTINUITY EQUATION

The resulting flux profile, however, does not necessarily satisfy the continuity equation (eq 2). Therefore, we iteratively change the μ^α profiles until the flux satisfies eq 2. The iteration procedure is based on the integral form of the continuity equation. The divergence theorem for the ith subvolume is

$$0 = \int_{\mathcal{D}_i} \nabla\cdot\mathbf{j}^{\alpha}(\mathbf{r})\,dV = \oint_{\mathcal{S}_i} \mathbf{j}^{\alpha}(\mathbf{r})\cdot\mathbf{n}(\mathbf{r})\,da \tag{6}$$

where $\mathcal{S}_i$ denotes the closed surface of volume element $\mathcal{D}_i$ and $\mathbf{n}(\mathbf{r})$ is the outward normal vector to the surface at point $\mathbf{r}$. The surface $\mathcal{S}_i$ is decomposed into subsurfaces (we call them faces), with which subvolume $\mathcal{D}_i$ meets the neighboring subvolumes $\mathcal{D}_j$. These faces will be denoted by $\mathcal{S}_{ij}$. The values of the concentration and the electrochemical potential on the face $\mathcal{S}_{ij}$ are computed by interpolation from the $\{c_i^\alpha\}$ and $\{\mu_i^\alpha\}$ values in the neighboring subvolumes on the two sides of $\mathcal{S}_{ij}$.

dx.doi.org/10.1021/ct2007988 | J. Chem. Theory Comput. 2012, 8, 824−829

We perform a linear interpolation between the centers of the neighboring subvolumes and use the resulting value for the whole face that separates these two subvolumes. Therefore, the values of the concentration, the electrochemical potential, its gradient, and the normal vector can be characterized by single values on the faces: $\hat{c}_{ij}^{\alpha}$, $\hat{\mu}_{ij}^{\alpha}$, $\nabla\hat{\mu}_{ij}^{\alpha}$, and $\mathbf{n}_{ij}$, respectively (it is practical to define subvolumes confined by flat faces). The diffusion coefficients must also be provided on the faces: $\hat{D}_{ij}^{\alpha}$. The surface integral in eq 6 then can be written as a sum over the faces:

$$0 = \sum_{j,\mathcal{S}_{ij}\in\mathcal{S}_i} \hat{\mathbf{j}}_{ij}^{\alpha}\cdot\mathbf{n}_{ij}a_{ij} \tag{7}$$

where $\hat{\mathbf{j}}_{ij}^{\alpha}$ is the flux density on the face $\mathcal{S}_{ij}$ of area a_{ij}. The iteration algorithm can be summarized as follows:

(1) An initial guess must be given for the discretized electrochemical potential profiles: $\{\mu_i^{\alpha}[1]\}$ (iterations will be denoted by numbers in square brackets). *In the first step*, we prescribe the concentrations on the boundary of the system (usually, in the left- and right-hand side baths: $c^{\alpha,\mathrm{L}}$ and $c^{\alpha,\mathrm{R}}$). Then, we calculate the chemical potentials $\mu_c^{\alpha,\mathrm{L}}$ and $\mu_c^{\alpha,\mathrm{R}}$ (see eq 3) that correspond to the prescribed concentrations using the Adaptive GCMC (A-GCMC) method of Malasics and Boda.[19] *In the second step*, we add the interactions with the applied potentials on the boundaries of the system, $z^{\alpha}e\Phi^{\mathrm{L}}$ and $z^{\alpha}e\Phi^{\mathrm{R}}$, where Φ^{L} and Φ^{R} are the Dirichlet boundary condition. The values of the electrochemical potential in the centers $\mathbf{r}_i$, $\mu_i^{\alpha}[1]$, are obtained by (properly guessed) interpolation between their values at the boundaries of the system. One possible choice for this interpolation will be given in the Results section.

(2) LEMC simulations are performed for all of the subvolumes using the $\{\mu_i^{\alpha}[1]\}$ values as input. The concentrations obtained from the simulations are denoted by $\{c_i^{\alpha}[1]\}$. Using $\{c_i^{\alpha}[1]\}$ with $\{\mu_i^{\alpha}[1]\}$ in the NP equation results in flux densities that do not necessarily satisfy eq 2.

(3) The electrochemical potential profiles for the next iteration, $\{\mu_i^{\alpha}[2]\}$, are obtained by assuming that together with $\{c_i^{\alpha}[1]\}$ in the NP equation they provide flux densities that satisfy eq 2. Substituting the NP equation for $\hat{\mathbf{j}}_{ij}^{\alpha}$ in eq 7, for a general $[n] \rightarrow [n+1]$ iteration, we obtain

$$0 = \sum_{j,\mathcal{S}_{ij}\in\mathcal{S}_i} \hat{D}_{ij}^{\alpha}\hat{c}_{ij}^{\alpha}[n]\nabla\hat{\mu}_{ij}^{\alpha}[n+1]\cdot\mathbf{n}_{ij}a_{ij} \tag{8}$$

Because $\hat{\mu}_{ij}^{\alpha}[n+1]$ is obtained from the $\mu_i^{\alpha}[n+1]$ values (and, also, $\hat{c}_{ij}^{\alpha}[n]$ from the $c_i^{\alpha}[n]$ values) by linear interpolation, eq 8 represents a system of N linear equations with $\{\mu_i^{\alpha}[n+1]\}$ being the unknowns for a given ionic species α. This system of linear equations can be converted into a matrix equation with a sparse matrix. Here, we used full-matrix methods to solve the system, but for large N, sparse-matrix methods can be used. This potentially allows the solution time to scale as an order of N, a strength of the NP+LEMC method.

(4) The new electrochemical potential profiles, $\{\mu_i^{\alpha}[n+1]\}$, are used in the LEMC simulations in the next, $[n+1]$th, iteration. These simulations provide new concentration profiles, $\{c_i^{\alpha}[n+1]\}$, and the iteration continues until convergence is achieved.

Note that perfect convergence is not possible due to statistical errors in the simulation results, $\{c_i^{\alpha}[n]\}$. As we will see, the iteration converges to the final result quite fast, and after that the data just fluctuate around certain mean values. These fluctuations are smaller if we run longer LEMC simulations in the iterations. We found it, however, more efficient to run shorter simulations and to average the results obtained in the iterations over the fluctuation period. The running average obtained this way can achieve arbitrary accuracy as the number of iterations increases.

4. RESULTS

Actual implementations of the procedure will be shown for two geometries.

(1) In the first test system, the ions diffuse through a membrane. The system has a planar symmetry. Therefore, the resulting profiles are one-dimensional: they depend only on the distance perpendicular to the membrane. This geometry makes it possible to illustrate our methodology more clearly and to compare with PNP/DFT.

(2) In the other test system, the ions diffuse through a pore spanning a membrane that separates two bulk electrolytes. The model pore is designed to be rotationally symmetric (the boundary conditions must also be rotationally symmetric). Therefore, the profiles are two-dimensional: they depend on the axial distance through the pore and the radial distance from the axis. This geometry makes it possible to illustrate the efficiency of our method for a more complex geometry.

We describe the models concisely and present results that are sufficient to illustrate our method. More details are provided in the Supporting Information.

4.1. Planar Geometry: Ions Diffusing through a Membrane. The ions travel in the x dimension, while the system is homogeneous in the y and z dimensions, which is achieved by applying periodic boundary conditions in these two dimensions in the LEMC simulations. There is a membrane between a 1 M NaCl electrolyte on the right-hand side and a 0.1 M NaCl electrolyte on the left-hand side. Ions are modeled as charged hard spheres with the Pauling radii for Na^+ and Cl^-, respectively, immersed in an implicit solvent characterized by a dielectric continuum of dielectric constant 78.5 at a temperature of 298.15 K. The probability that an ionic species α enters the membrane is tuned by an energy penalty in the membrane. The fact that the mobility of the ions is smaller in the membrane than in the bulk is taken into account by reducing the diffusion coefficients by a factor 10.

Boundary conditions are that the electrochemical potential is $\mu^{\alpha,\mathrm{L}} = \mu_c^{\alpha,\mathrm{L}} + z^{\alpha}e\Phi^{\mathrm{L}}$ on the left-hand side, while it is $\mu^{\alpha,\mathrm{R}} = \mu_c^{\alpha,\mathrm{R}} + z^{\alpha}e\Phi^{\mathrm{R}}$ on the right-hand side bulk for species α. The bulk chemical potentials, $\mu_c^{\alpha,L}$ and $\mu_c^{\alpha,\mathrm{R}}$ corresponding to the prescribed concentrations 0.1 and 1 M were calculated with the A-GCMC method.[19] The electrical potential in the left bath is chosen to be $\Phi^{\mathrm{L}} = 0$, so the value Φ^{R} (20 mV = $0.778e/kT$, in this work) gives the voltage.

Due to the planar symmetry, the subvolumes are slabs with two faces. Equation 8 then expresses that whatever enters through the left face of the slab, it leaves through the right face of the slab. The details are found in the Supporting Information.

We show how the $\mu^{\alpha}(x)$ profiles converge during the iteration in Figure 1. The initial guess ($n = 1$) for the chemical potential profiles is that $\mu_c^{\alpha}(x)$ is constant in the bulk regions and drops

dx.doi.org/10.1021/ct2007988 | J. Chem. Theory Comput. 2012, 8, 824−829

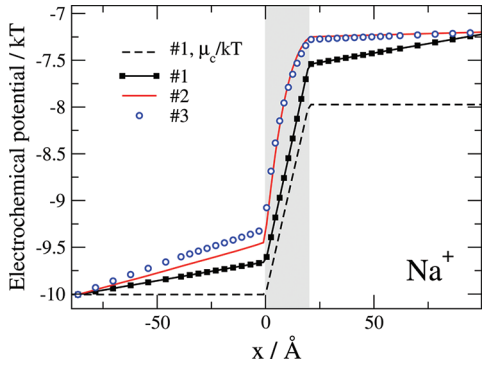

Figure 1. Convergence of the electrochemical potential of Na^+ through two iterations for the planar geometry. The dashed line is the initial guess for $\mu_c^\alpha(x)$, while the curve labeled with #1 is the initial guess for $\mu^\alpha(\mathbf{r})$. The curves labeled with #2 and #3 are the updated $\mu^\alpha(x)$'s obtained in the first and second iterations.

linearly in the membrane region (dashed line in Figure 1). The initial guess for the $\mu^\alpha(x)$ is obtained by adding the interaction with the applied field (filled black squares with solid line in Figure 1). The trivial solution of Laplace's equation for the planar geometry is that $\Phi^{appl}(x)$ drops linearly between the boundaries of the system. This choice for $\mu_i^\alpha[1]$ ensures that the boundary conditions for the electrochemical potential are fulfilled. The algorithm converges fast after only three iterations with relatively short (2×10^6 sampled configurations) simulations for each iteration (Figure 1). The updated μ^α(x) from the third iteration (#4) and that from the second iteration (#3) would be indistinguishable on the scale of the figure.

The electrical potential profiles obtained in the first iteration and the final averaged result are shown in Figure 2 in

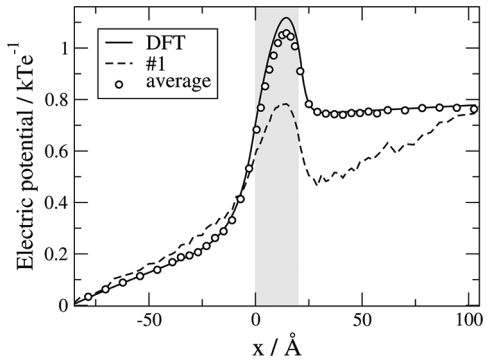

Figure 2. The mean electrical potential profile obtained from the first iteration (dashed line) and as an average from 10 iterations (symbols) for the planar geometry. The solid line shows the PNP/DFT result.

comparison with the PNP/DFT curve (more curves showing convergence are found in the Supporting Information). The potential obtained from a single (relatively short) simulation is quite noisy, while the converged and averaged result is smooth and shows excellent agreement with the PNP/DFT results. This agreement indicates that the two methods do the same thing although with different accuracies.

The converged potential profile is quite flat in the 1 M region to the right from the membrane because the electrical resistance in this region is small (due to the large concentration of charge carriers). The 0.1 M bulk region, on the other hand, is a high-resistance element. In the membrane region, the electrical potential shows nonmonotonic behavior, resulting in a possibly negative electrical resistance. In this region, therefore, the total driving force (the drop of the electrochemical potential) should be used to measure the resistance of this region. Figure 1 shows that the drop of $\mu^\alpha(x)$ is largest in the membrane region, indicating that this region has the largest resistance to the flow of ions driven by the electrochemical potential gradient (due to the reduced diffusion coefficients in the membrane).

The electrical potential profile is a sum of $\Phi^{appl}(x)$ and the potential produced by the ionic distributions. A charge separation occurs in and near the membrane forming electrical double layers as seen in Figure 3, where the distribution of ions

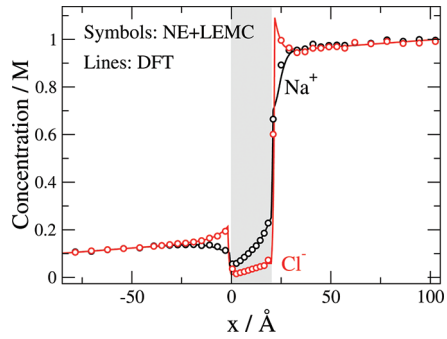

Figure 3. Concentration profiles for Na^+ and Cl^- as obtained from the NP+LEMC (symbols) and the PNP/DFT (curves) methods for the planar geometry.

as obtained from the NP+LEMC and the PNP/DFT methods is shown (concentration profiles in various iterations are shown in the Supporting Information). These double layers produce an electric field that counter-balances the applied field and produces the profiles in Figure 2 (the flat potential in the 1 M bulk, for example).

The fluxes that are computed with $c^\alpha[n]$ and $\mu^\alpha[n]$ (i.e., before updating) are not constant (as they should be in this geometry), but they flatten out as the iteration proceeds (see Supporting Information). The fluxes that are computed with $c^\alpha[n]$ and $\mu^\alpha[n+1]$ (i.e., the updated chemical potential), on the other hand, are constant by design. These values also fluctuate around a mean value. Their average provides the final result for the fluxes carried by the various ions.

4.2. Rotational Geometry: Ions Diffusing through a Pore. A membrane generally contains pores through which particles travel from one side to the other. Biological ion channels are an example. In this work, we test our method on a pore geometry that we used in our equilibrium GCMC simulations for ion channels.[20] The pore (of radius 5 Å) spans a membrane of thickness 20 Å. It has a 10 Å central cylindrical region sandwiched by two vestibules on the two sides (for details, see the Supporting Information). Negative partial charges are placed on the wall of the central cylinder on three concentric rings, thus forming a pore with $-3e$ structural charge.

The boundary conditions are the same as in the planar symmetry except that they are now set on the surface of a large cylinder (72 Å in length and 30 Å in radius) surrounding the pore region: the left-hand side boundary conditions are prescribed on the left part of the cylinder left from the membrane, while the right-hand side boundary conditions are prescribed on the right part of the cylinder right from the membrane. The solution of the Laplace equation now requires a numerical procedure; we used a boundary element method[20] to compute the surface charges on the system's boundary. The potential inside the cylinder in the

dx.doi.org/10.1021/ct2007988 | J. Chem. Theory Comput. 2012, 8, 824−829

subvolumes' centers was considered as that produced by these surface charges.

The subvolumes in this case are squares in the (x,r) plane, where the x axis is in the centerline of the pore and r is the distance from it. In three dimensions, these squares are rings. The problem, however, can be handled in two dimensions, and eq 8 contains a sum over four faces: ions can travel through faces to the left, right, up, and down. The equations can be found in the Supporting Information.

The diffusion constant was considered to be the same in the bulk and in the pore. Although the mobility of ions is reduced in pores and confined geometries, we defer the study of this effect to later papers, where we will apply the NP+LEMC technique to ion channels and synthetic nanopores.

The results of the calculations are now surfaces over the (x,r) plane. The initial condition of the $\mu^{\alpha}(x,r)$ surface for Na^+ (labeled as #1) is shown in Figure 4. It is a linear interpolation

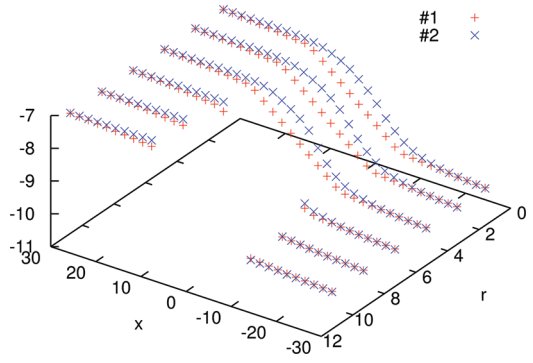

Figure 4. Electrochemical potential of Na^+ for the pore geometry. The red + symbols show the initial guess, while blue × symbols show the updated $\mu^{\alpha}(x,r)$ obtained in the first iteration.

in the pore region ($|x| < 10$ Å) similar to the planar symmetry (see Figure 1). The surface obtained after an iteration (labeled as #2) is also shown. The surface from the next iteration is very close to the #2 surface, so the convergence of the iteration is quite fast. The region without data is the membrane, where the concentration of Na^+ is zero (it is indicated with shaded gray areas in Figures 5 and 6). The subvolumes in this region are not included in eq 8.

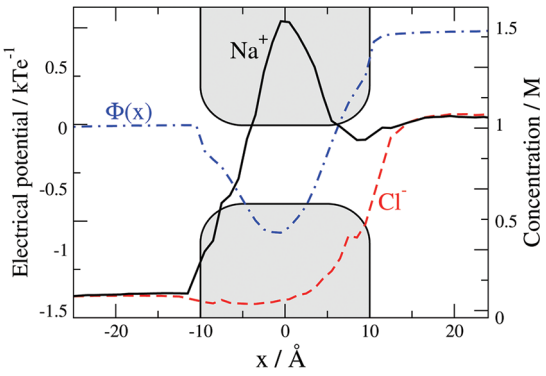

Figure 5. The concentrations of Na^+ and Cl^- ions (right axis) and the mean electrical potential (left axis) as functions of the axial distance through the pore averaged over the cross-section of the permeation pathway of the ions.

Plotting and digesting such surfaces is a difficult task, so it is often advantageous to plot profiles that are averaged over one

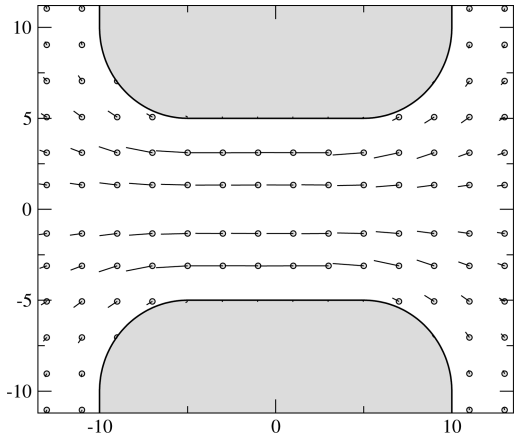

Figure 6. The flux densities of Na^+ ions in the pore geometry. The lengths of dashes are proportional to the magnitudes of the flux densities in the given positions (indicated by circles), while their directions correspond to the flux density vectors' directions. Only a part of the whole simulation domain is shown.

dimension. Figure 5 shows the concentration profiles and the electrical potential profile averaged over the cross-section through which the ions permeate. The presence of negative structural charges makes the pore cation selective, as indicated by the Na^+ vs Cl^- profiles. The Na^+ ions cannot balance the structural charges in the confined space of the pore; therefore, the charge of the pore is overall negative (the structural charges are balanced from outside). This produces a negative potential well as indicated by the dot-dashed line in Figure 5.

Since the flux densities are vector quantities, it is convenient to illustrate them with actual vectors as shown in Figure 6. The figure clearly shows the lines along which the diffusion of Na^+ ions occurs.

5. CONCLUSIONS

The proposed mechanism of LEMC simulations coupled to the NP equation provides an efficient way to study steady-state flux in systems modeled on the molecular level. It is applicable not only to implicit solvent electrolytes but also to systems modeled on the all-atom level. At high densities, particle insertions and, thus, GCMC sampling become inefficient, but that can be overcome with various methods that improve sampling (e.g., cavity biased sampling). The method is equally applicable to the diffusion of uncharged particles. In this case, ionic charges, electrical potential, and Poisson's equation do not appear in the formalism, and we just iterate the usual chemical potential.

Despite these constraints, however, the NP+LEMC technique has several significant advantages over other methods that can make it an important tool in a wide variety of applications. Compared to approximate theories like DFT, the LEMC simulation provides the same information as DFT, but it can be applied to three-dimensional systems with a much wider variety of geometries and pair potentials and provides exact results (apart from statistical and system size errors). Moreover, it provides a mean electrical potential that automatically satisfies Poisson's equation, while an additional loop is required in PNP and PNP/DFT to make the calculations electrostatically self-consistent.

We use a lattice to discretize the variables of the NP equation. This resembles the way Lattice Kinetic Monte Carlo (LKMC) handles the problem of diffusion.[21] There is an important difference, however. Our LEMC simulations are continuous in

the sense that particles can be inserted/displaced at any position of the simulation domain, while the dynamics is taken care of by the (discretized) NP equation. LKMC, on the other hand, simulates dynamics directly by allowing ion hopping between lattice cells with well-defined probabilities. Nonlattice-based MC methods include the DMC technique,[14,15] where random and continuous particle displacements are allowed (not only hops) and moves are accepted/rejected on the basis of the system's energy computed from the interparticle potentials. KMC algorithms without restrictions to lattice sites have also been described.[22]

The advantage of these and other direct dynamical particle simulations like MD and BD is that these simulations provide dynamics and do not require external information about the diffusion coefficient. In the NP+LEMC technique, we need to provide the diffusion coefficient profiles, which are generally not known but can be fit to experimental data.[23−25] Another advantage of the direct simulation methods is that they can be applied to problems where momentum exchange occurs (single file ion transport through narrow ion channels, for example). The NP+LEMC technique, on the other hand, assumes drift-diffusion and can be used only if the NP equation is valid. Furthermore, our technique, in its present form, is designed to study steady-state diffusion and cannot be applied for time-dependent processes.

The advantage of the NP+LEMC method, however, is that it provides converged results very quickly. The LEMC method samples only the configurational space (positions of particles), while dynamical methods sample phase space (positions and velocities of particles). Sampling only the configurational space can be performed more efficiently because the advantageous sampling capabilities of the equilibrium MC techniques can be exploited. Dynamical methods, on the other hand, cannot always sample trajectories for a long enough time to compute flux adequately (KMC can be a good alternative here with its stochastic approach).

Moreover, because it uses the GC ensemble, NP+LEMC can be used on systems with very low concentrations (e.g., 10^{-6} M and below). In contrast, simulation methods that use fixed numbers of particles cannot even reach 10^{-3} M concentrations efficiently. This is important in many applications like nanofluidic devices with charged walls where low concentrations are used to exclude co-ions to improve ion separation and pressure-to-voltage energy conversion.[26] At the same time, ion size is important even at low concentrations in such a system for nonlinear effects like charge inversion.[27] Low concentrations are also vital in biological applications where Ca^{2+} and Mg^{2+} concentrations range between 10^{-7} and 10^{-3} M. Equally important in biological systems is the application of small voltages (0−100 mV) that is difficult to do in other particle simulation methods but straightforward in NP+LEMC.

The need to apply simulation methods to mesoscopic systems on the nanometer length scale and above is continuously increasing. The NP+LEMC method applied to coarse-grained models is a promising tool to study diffusive particle transport in systems that are beyond the microscopic length scale. Therefore, NP+LEMC is a powerful and very general new technique that will give physical insight into a wide variety of systems.

■ ASSOCIATED CONTENT

Supporting Information

A more detailed description of the test systems shown in the Results section and additional results that show how our iterative procedure works. This information is available free of charge via the Internet at http://pubs.acs.org.

■ AUTHOR INFORMATION

Corresponding Author

*E-mail: boda@almos.vein.hu.

Notes

The authors declare no competing financial interest.

■ ACKNOWLEDGMENTS

This material is based on work supported by, or in part by, the U.S. Army Research Laboratory and the U.S. Army Research Office under Contract No. W911NF-09-1-0488 to D.G. The support of the Hungarian National Research Fund (OTKA K75132) to D.B. is acknowledged. We are grateful to Dr. Tamás Kristóf for inspiring discussions. The present publication was realized with the support of the project TÁMOP-4.2.2/B-10/1-2010-0025.

■ REFERENCES

(1) Chen, D.; Lear, J.; Eisenberg, B. *Biophys. J.* **1997**, *72*, 97−116.
(2) Gillespie, D.; Nonner, W.; Eisenberg, B. *J. Phys.: Condens. Matter* **2002**, *14*, 12129−12145.
(3) Allen, M. P.; Tildesley, D. J. *Computer Simulation of Liquids*; Oxford: New York, 1987.
(4) Frenkel, D.; Smit, B. *Understanding Molecular Simulations*; Academic Press: San Diego, CA, 1996.
(5) Kreuzer, H. J. *Nonequilibrium Thermodynamics and its Statistical Foundations*; Clarendon Press: Oxford, U. K., 1981.
(6) de Groot, S. R.; Mazur, P. *Non-Equilibrium Thermodynamics*; Dover: New York, 1984.
(7) Tschoegl, N. W. *Fundamentals of Equilibrium and Steady-State Thermodynamics*; Elsevier: Amsterdam, 2000.
(8) Evans, D. J.; Morriss, G. *Statistical Mechanics of Nonequilibrium Liquids*; Cambridge University Press: New York, 2008.
(9) Bortz, A.; Kalos, M.; Lebowitz, J. *J. Comput. Phys.* **1975**, *17*, 10−18.
(10) Gillespie, D. T. *J. Comput. Phys.* **1976**, *22*, 403−434.
(11) Gillespie, D. T. *J. Phys. Chem.* **1977**, *81*, 2340−2361.
(12) Gilmer, G. H. *Science* **1980**, *208*, 355−363.
(13) Voter, A. F. *Phys. Rev. B* **1986**, *34*, 6819−6829.
(14) Rutkai, G.; Kristóf, T. *J. Chem. Phys.* **2010**, *132*, 124101.
(15) Rutkai, G.; Boda, D.; Kristóf, T. *J. Phys. Chem. Lett.* **2010**, *1*, 2179−2184.
(16) Heffelfinger, G. S.; van Swol, F. *J. Chem. Phys.* **1994**, *100*, 7548−7552.
(17) Lísal, M.; Brennan, J. K.; Smith, W. R.; Siperstein, F. R. *J. Chem. Phys.* **2004**, *121*, 4901−4912.
(18) Im, W.; Seefeld, S.; Roux, B. *Biophys. J.* **2000**, *79*, 788−801.
(19) Malasics, A.; Boda, D. *J. Chem. Phys.* **2010**, *132*, 244103.
(20) Boda, D.; Valiskó, M.; Eisenberg, B.; Nonner, W.; Henderson, D.; Gillespie, D. *J. Chem. Phys.* **2006**, *125*, 034901.
(21) Flamm, M. H.; Diamond, S. L.; Sinno, T. *J. Chem. Phys.* **2009**, *130*, 094904.
(22) Henkelman, G.; Jonsson, H. *J. Chem. Phys.* **2001**, *115*, 9657−9666.
(23) Gillespie, D. *Biophys. J.* **2008**, *94*, 1169−1184.
(24) Gillespie, D.; Boda, D. *Biophys. J.* **2008**, *95*, 2658−2672.
(25) Boda, D.; Valiskó, M.; Henderson, D.; Eisenberg, B.; Gillespie, D.; Nonner, W. *J. Gen. Physiol.* **2009**, *133*, 497−509.
(26) van der Heyden, F. H. J.; Bonthuis, D. J.; Stein, D.; Meyer, C.; Dekker, C. *Nano Lett.* **2006**, *6*, 2232−2237.
(27) van der Heyden, F. H. J.; Stein, D.; Besteman, K.; Lemay, S. G.; Dekker, C. *Phys. Rev. Lett.* **2006**, *96*, 224502.